Study of damage generation induced by focused helium ion beam in silicon

Rongrong Li,[1] Rui Zhu,[2,a)] Shulin Chen,[2] Chao He,[2] Mingqiang Li,[2] Jingmin Zhang,[2] Peng Gao,[2,3,4] Zhimin Liao,[1,b)] and Jun Xu[2]
[1]*State Key Laboratory for Mesoscopic Physics, School of Physics, Peking University, Beijing 100871, China*
[2]*Electron Microscopy Laboratory, School of Physics, Peking University, Beijing 100871, China*
[3]*Collaborative Innovation Center of Quantum Matter, Beijing 100871, China*
[4]*International Center for Quantum Materials, School of Physics, Peking University, Beijing 100871, China*

(Received 20 March 2019; accepted 30 April 2019; published 17 May 2019)

Helium ion microscope (HIM) has presented an outstanding ability to image and nanofabricate thin film and two-dimensional materials with high precision. However, the concomitant damage and implantation induced by focused helium ion beam should influence the imaging quality and nanomachining efficiency inevitably, especially for bulk samples. In this work, the authors investigated the generation process of damages at nanoscales in single crystalline bulk silicon caused by ions implantation in HIM using transmission electron microscopy. The dependence of implantation and damage on ion dose, ion energy, and beam current was also discussed and analyzed. It was found that the damage should be originated from the local defects caused by ion implantation and the crystal structure could be gradually destroyed and transform into amorphous silicon with the generation and growth of subsurface nanobubbles as ion dose increased. The local concentration of implanted helium ion was found as a universal factor to impact on the damage level and the size of nanobubbles directly. These findings not only shed lights on the effective imaging and nanofabrication of HIM but also provide a further understanding in the nuclear irradiation area. *Published by the AVS.* https://doi.org/10.1116/1.5096908

I. INTRODUCTION

Helium ion microscope (HIM) has been applied successfully in subnanometer resolution imaging and nanoscale fabrication due to its unique imaging contrast and small probe size of 0.24 nm.[1–3] For suspended nanofilms and two-dimensional (2D) materials, HIM works well in generating nanostructures, such as precise controlled fabrication of nanopore, nanomesh, and nanoribbon with a size down to several nanometers on suspended graphene[4–7] and molybdenum disulfide (MoS_2)[8] as well as carbon nanomembranes[4] and silicon nitride membranes.[4,9] Ion beam sculpting of freestanding semiconductor nanowires with sub-10 nm features has also been reported.[10]

However, for bulk materials or substrate-based structures, HIM usually induces subsurface implantation and damages due to the low sputter yield and diffusivity of the helium ions,[3,11,12] such as nanobubbles and structure damages, which greatly restrict the application of HIM in nanomachining. Thus, numerous efforts were devoted to understanding and solving these problems. It has been shown by Livengood *et al*. how helium ions induced damage evolves with increasing ion dose.[3] In addition, helium ions–silicon (Si) interactions in both bulk and film structures were systematically studied by Tan's group;[13] furthermore, pulsed laser annealing and gas-assisted process were introduced to reduce the implantation and enhance the material removal rate.[14,15] Another experiment showed that the helium ion diffusion in bulk materials could be enhanced by *in situ* heating.[16] These investigations helped us to understand the helium ion induced damage from different points of view and provided some guidelines on a wide range of precise nanofabrication regimes of HIM. However, so far, the mechanism of helium bubble formation remains to be elucidated.

Here, from a very basic point of view, we expatiated the mechanism of focused helium ion beam (FHIB) induced lattice damages and nanobubbles generation in single crystalline silicon, a standard semiconductor material. To characterize the damage process precisely, we adopted a single spot and a single-pixel line irradiation under a different ion dose, beam energy, and beam current using HIM. The cross-section samples obtained using focused ion beam (FIB) system with *in situ* lift-out technique were analyzed by transmission electron microscopy (TEM) and aberration-corrected scanning TEM. In this way, the process of damage formation could be resolved with atomic resolution. The local ion concentration was analyzed with respect to ion dose, beam energy, and beam current and found to be the determined factor in the process of damage generation. This work provides a detailed and fundamental understanding about the interaction between focused helium ion beam and single crystalline Si and helps to promote the applications of HIM.

II. EXPERIMENTAL METHODS

A. Sample description

The single crystalline Si used in this work was Czochralski (CZ)-grown N-doped Si (111) wafer with a resistivity of 0.003–50 Ω cm. Before ion irradiation by HIM, the samples were ultrasonic cleaned in acetone, isopropyl alcohol, and deionized water for 10 min in sequence and

[a)]Electronic mail: zhurui@pku.edu.cn
[b)]Electronic mail: liaozm@pku.edu.cn

further cleaned by argon (Ar) plasma of 80 W for 3 min. Directly thereafter, they were loaded into the HIM chamber and processed by *in situ* moderate plasma cleaning for 1 h. All these above were to ensure the cleanliness of the samples and HIM chamber and to avoid hydrocarbon contamination in the following helium ion milling process.

B. Helium milling process

An HIM (Zeiss Orion NanoFab) was used to generate FHIB and make it irradiate on the Si surface in a single spot or along a single-pixel line. To avoid additional ion implantation, the regions to be irradiated were not observed by HIM. During the irradiation process, a series of parameters were regulated controllably. The ion dose was set conveniently to predesigned values by ZEISS NPVE software. Beam energies of 12 and 30 keV were selected here in order to make a comparison in different energy cases, while beam current was varied from 0.5 to 5 pA by adjusting helium pressure. Only one variable parameter was controlled in each group of experiments which included five milling points or lines in a row with another two marks at both ends in order to obtain the cross-sectional image of middle implant sites in the following TEM lift-out process.

C. TEM sample lift-out process and characterization

A FIB system (FEI STRATA DB235) was utilized to prepare standard TEM cross-section samples of irradiated regions by lift-out technique for further analysis. In order to prevent additional damages induced by Ga ion beam during TEM sample preparation process, a 20 nm carbon layer and a Pt or Cr or Au layer with several tens of nanometers were first deposited on the FHIB-irradiated silicon surface by a precision etching coating system (GATAN Model 682). Then another Pt/C layer of about 1 μm was prepared by Ga ion beam induced deposition. After the lift-out process, the cross section of FHIB-irradiated areas were characterized by Tecnai F20 at 200 kV and aberration-corrected FEI Titan Themis G2 microscope at 300 kV.

III. RESULTS AND DISCUSSION

A. Impact of implantation dose on the damage process

In this section, we present the damages on Si crystal structure created by irradiation of scanning FHIB at various doses. Characterization results clearly reveal the progression of the defect and nanobubbles formation with increasing dose, which provides a distinct understanding about how the ion dose impacts the damage process at nanoscales.

Single spot irradiation without scanning was introduced to observe the helium ion implantation process. These experiments were conducted with ion dose ranging from 1.9×10^8 to 3.9×10^8 ions at the beam energy of 30 keV and beam current of 1.50 pA. The unit of implantation dose was represented by the number of ions per single-pixel point or spot area. Figure 1 shows the cross section of the injected region in crystalline Si with an implantation dose of 1.9×10^8 ions. It could be observed that the deposited Pt layer appear a dark contrast above the sample surface in Fig. 1(a). There existed an amorphous Si layer indicated between two dotted straight lines with a thickness of about 40 nm created by 30 keV Ga ion beam milling during the lift-out process. The injected area appeared brighter than the original Si crystal area according to the corresponding bright field image [Fig. 1(a)]. Nevertheless, the original crystal structure was still preserved in the implanted region, as shown in Fig. 1(b). The selected area electron diffraction (SAED) in the area denoted by the black square in Fig. 1(a) suggests that the injected helium

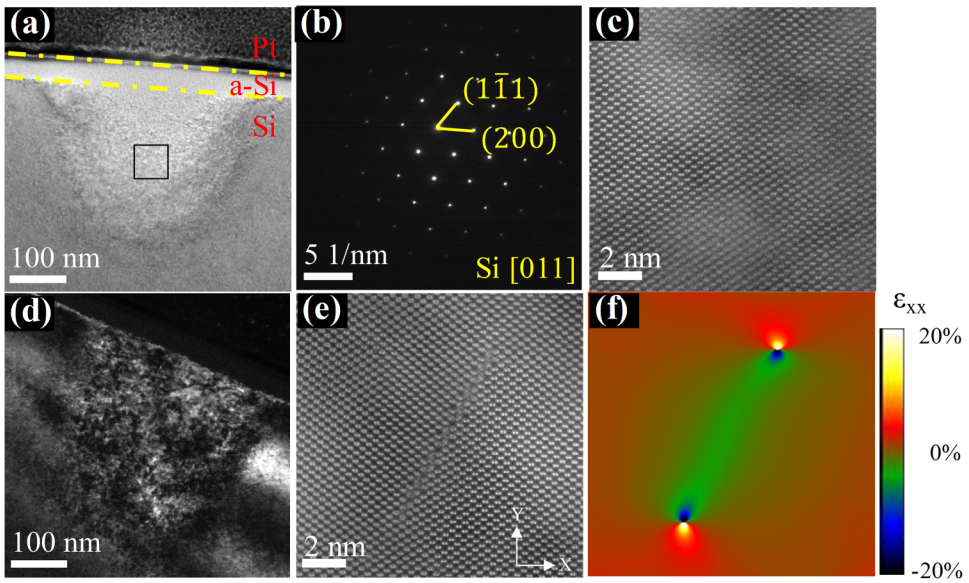

FIG. 1. Cross-sectional TEM images of silicon sample scanned by a single-pixel point with a helium ion dose of 1.9×10^8 ions at the beam energy of 30 keV (a) The bright field TEM image of the implant area; (b) selected area electron diffraction of the area marked in (a); (c) HAADF image in the area marked in (a); (d) dark field TEM image corresponding to (a); (e) HAADF image of a defect in the implanted area; and (f) calculated strain field (ε_{xx}) in the horizontal direction according to (e). A positive value means relative tensile strain while a negative value means relative compressive strain.

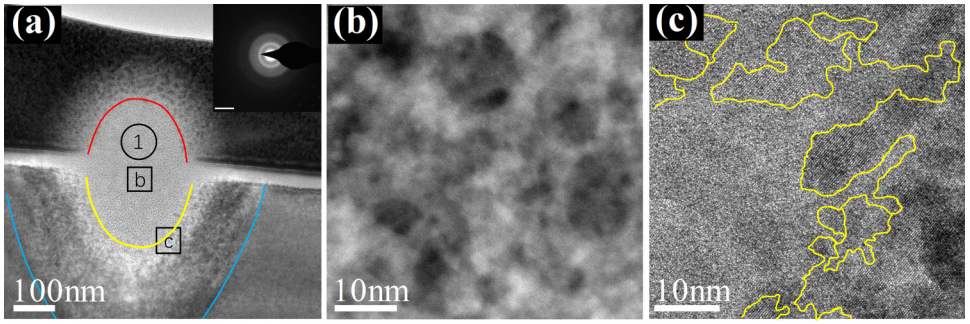

FIG. 2. TEM cross-section images of silicon sample scanned by a single-pixel point with a helium ion dose of 2.9×10^8 ions at the beam energy of 30 keV (a) The bright field image of the inject area. The inset image shows the electron diffraction pattern of the selected area in position (1) and the scale bar is 5 1/nm. (b) HAADF image of the area with nanobubbles marked in (a). (c) High resolution TEM image of the transition boundary indicated by the curved line between the crystalline region and the amorphous region marked in (a).

ions could not destroy the crystal structure efficiently at the implantation dose of 1.9×10^8 ions. Furthermore, the high angle annular dark field (HAADF) image in Fig. 1(c) illustrated one region without detectable damages. However, numerous structural defects were recognized from the intercrossed bright and dark contrast of the implantation area in the dark field image [Fig. 1(d)]. The defects, such as vacancies, interstitials, and dislocations, should result from the displacements of Si atoms that were collided with high energy helium ions. Although the atomic structures of the defects were difficult to observe in the cross-sectional TEM sample with an implantation dose of 1.9×10^8 ions, one dislocation-like defect was identified and demonstrated by the HAADF image shown in Fig. 1(e). According to the atomic-scale image, the strain field distribution shown in Fig. 1(f) was extracted by the geometrical phase analysis (GPA).[17] Here, ε_{xx}, the direct strain in the horizontal direction (the x direction), was illustrated. It could be seen that relative compressive strain ($\varepsilon_{xx} < 0$) exists nearby the defect and relative tensile strain ($\varepsilon_{xx} > 0$) was around the defect, especially at both ends of the defect. It suggests that the defects caused by low dose ions injection would lead to lattice strain and distortions, which, in turn, explicated the contrast distribution in the dark field image shown in Fig. 1(d).

Figure 2 shows the irradiated area of 2.9×10^8 ions injection dose. The Si crystal lattices were damaged and transformed to amorphous structure according to SAED image shown in Fig. 2(a). The middle concave line shows the interface between the amorphous region and the single crystalline region with defects like Fig. 1(a), while the concave lines on both sides indicates roughly the interface between the original single crystalline Si substrate and the injected area. An obvious swelling region appeared above the surface. The interface between swelling Si and protective layer with dark contrast, indicated by the top convex line in Fig. 2(a), was not sharp enough due to 30 keV Ga ion beam milling during the sample lift-out process. In the amorphous region as shown in HAADF image [Fig. 2(b)], there were several cavitylike structures, i.e., nanobubbles, with diameters from several to more than 10 nm. Moreover, it was clear that a few small cavities could be found behind the large ones.

As a result of the formation of nanobubbles, the density of the amorphous Si is highly decreased and the swelling appears above the surface. A detailed transition area between the amorphous region and the crystalline region is shown in Fig. 2(c). The winding transition boundaries were marked with curved lines. It was found that there were no cavities near the boundaries. Thus, the damages worsened from the interface to the center of the injected region.

With ions injection dose increased further, larger bubbles of about tens of nanometers were observed in TEM bright field image of the cross-sectional sample [Fig. 3(a)]. 60% of bubbles showed size within around 12.5–22.5 nm according to the statistical distribution of bubbles size shown in Fig. 3(b).

We could speculate that the damage is originated from the defects like vacancies induced by ion implantation. The vacancies tend to aggregate into vacancy clusters due to its high mobility,[18] which will lead to the strain field around the defects. It has been demonstrated that the tensile displacement field around vacancy clusters has the ability to attract helium atoms.[19] As a result, more and more disordered vacancy clusters form and aggregate, which leads to a gradual transformation of Si from crystalline to an amorphous state. And in the aggregation process, the formation of a kind of "helium atmosphere" is believed to occur eventually and the pressure increases with ions concentration.[19] Therefore, helium bubbles of about several nanometers will appear and grow if more ions are injected, resulting in the swelling above the sample surface and the decreasing of the implanted regions density.

It is worth comparing the damage process induced by He and Ga ion beam. Similarly, focused Ga ion beam (FGIB)

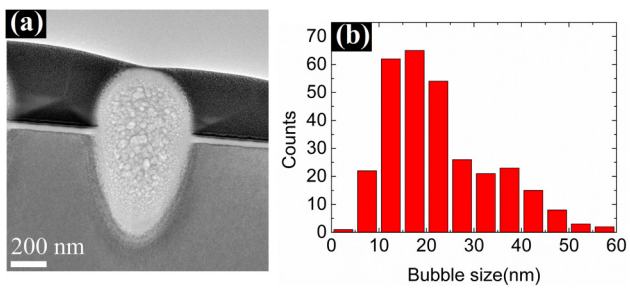

FIG. 3. Silicon sample scanned by a single-pixel point with a helium ion dose of 3.9×10^8 ions at the beam energy of 30 keV. (a) The bright field image of the cross-sectional inject area. (b) The statistical distribution of the nanobubbles diameter corresponding to (a).

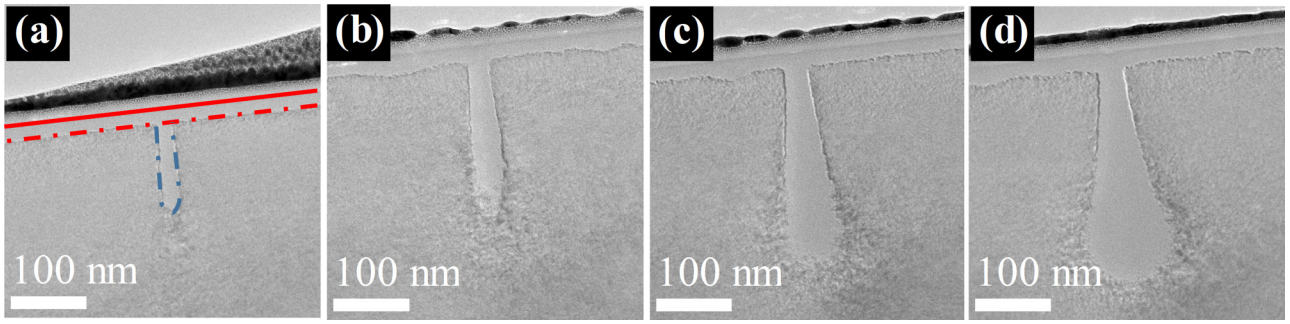

FIG. 4. TEM images of cross-section (111) silicon sample scanned as a single-pixel line with increasing helium ion dose (a) 0.003, (b) 0.006, (c) 0.009, and (d) 0.012 nC/μm at the beam energy of 30 keV and beam current of 1.6 pA.

can also lead to defects in the milling process, which causes a change in the strain field in the injecting region. The strain field could introduce more defects and weaken sputtering according to the MD simulation.[20] Differently, He ion is about 16.4 times lighter than Ga ion, and the Si sputtering yields with He and Ga ions are 0.0165 and 2.23 atoms/ion at 30 keV beam energy, respectively. Therefore, the amorphization induced by FGIB arises mainly from the combination of defects generation and removal of Si atoms.[21] For FGIB irradiation, the milled edge would not be sharp and contain the amorphous region with decreased density.[22] Also, it was speculated from the swelling of the FHIB-irradiated Si surface that the density of the amorphous region induced by He ion implantation also decreased. In order to mitigate the damage caused by FIB, the method that can reduce the strain of material and enhance the diffusion of ions may be useful, such as thermal treatment.[16,23]

B. Ion concentration

Normally, the implantation dose is defined as the particle number per area on the two-dimensional surface and usually used to characterize the intensity of ion implantation. Actually, the implantation should proceed in a three-dimensional domain. The dose is not sufficient to characterize the damage level or implantation concentration. The ion–matter interaction volume should be taken into account. In this section, the role played by implanted ions concentration in FHIB induced damages was investigated. Here, the ion concentration is defined as the number of implanted ions divided by interaction volume. For the convenience of measurement, FHIB scanned in a single-pixel line with original spot width and 1 μm length was performed to generate damage in Si, and the amorphous region is roughly considered to be interaction volume. The results show how the damaged area and the generation and growth of nanobubbles are affected by the ion dose and beam energy in the implant process. It was found that the generation and growth of helium bubble are primarily dependent on the local ion concentration.

Figure 4 shows the dependence of cross-sectional interaction area on ion dose with 1.6 pA beam current and 30 keV beam energy. A straight solid line in Fig. 4(a) indicates the sample surface. The carbon layer and Pt layer above the sample surface are described above. The straight dotted line shows the interface between the crystalline region and the amorphous layer created by 30 keV Ga ion beam milling during the lift-out process. The damage domain outlined by a curved dotted line in Fig. 4(a) appeared brighter in contrast than primary silicon, which resulted from a transformation from crystalline to amorphous Si. The domains become deeper and reshaped like droplet gradually with the dose increased from 0.003 to 0.012 nC/μm due to more ions implantation and scattering. The cross-sectional damage domain also becomes larger with increasing ion dose. According to Fig. 4, nanobubbles were not observed in the results discussed above due to the relatively low implantation dose, which was in accordance with the results in Sec. III A.

For a larger dose of 0.015 nC/μm and 30 keV beam energy, there were also no nanobubbles observed in the implanted sample from the cross-sectional TEM image shown in Fig. 5(a). However, nanobubbles of sub-10 nm were found distinctly in 12 keV FHIB implanted Si with the same implantation dose of 0.015 nC/μm and beam current of 1.6 pA as illustrated in Fig. 5(b). It could be observed that the penetration depth of 30 keV helium beam was about 300 nm, twice as deep as that of 12 keV beam, which is consistent with the stopping and range of ions in matter simulation, a group of programs which calculate the stopping and range of ions (10 eV–2 GeV /amu) into matter using a quantum mechanical treatment of ion-atom collisions.[3] The cross-sectional interaction domain at 30 keV beam energy looked more like a droplet with a width of about 140 nm, while it was nearly a round shape of about 130 nm diameter for 12 keV helium beam implantation, which could be understood by principle of

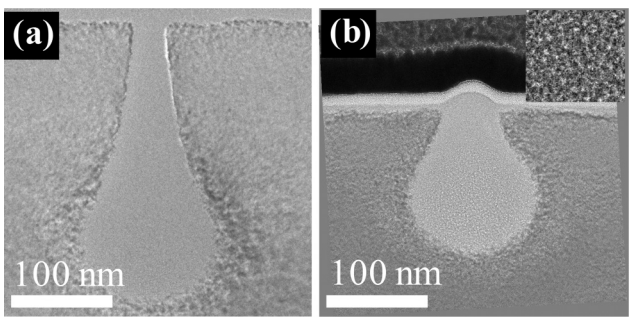

FIG. 5. TEM images of cross-section (111) silicon sample scanned as a single-pixel line at the beam energy of (a) 30 and (b) 12 keV with an ion dose of 0.015 nC/μm and a beam current of 1.6 pA. The inset image shows details of nanobubbles with a diameter of about 1.6 nm.

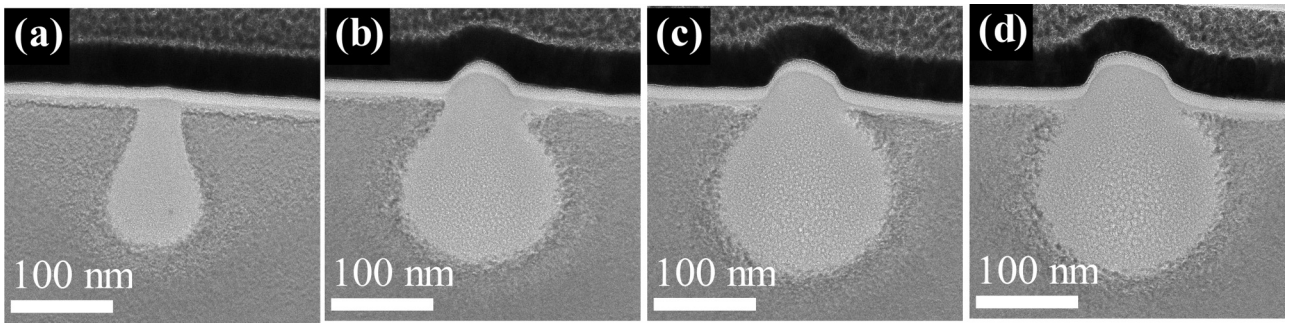

FIG. 6. TEM images of cross-section (111) silicon sample scanned as a single-pixel line with increasing helium ion dose (a) 0.008, (b) 0.023, (c) 0.030, and (d) 0.038 nC/μm at the beam energy of 12 keV and beam current of 1.6 pA.

Rutherford scattering.[24] The interaction domain areas for 30 and 12 keV FHIB discussed above were estimated to be 2.78×10^4 and 1.54×10^4 nm^2, respectively. Although the energy deposition at 30 keV was heavier than that at 12 keV, the helium ions deposition in Si of 30 keV FHIB should be more dispersive than that of 12 keV FHIB with the same dose owing to a larger interaction domain volume at 30 keV beam than at 12 keV. To quantitatively study FHIB induced damage, the deposited helium ion concentration was defined to characterize the average density of implanted helium ions in the total interaction domain. The calculated ion concentrations for 30 and 12 keV FHIB discussed above were 3.37 and 6.07 ions/nm^3, respectively.

To further confirm the results and study nanobubbles generation induced by a low energy beam, a set of doses from 0.008 to 0.038 nC/μm were introduced in implantations with 12 keV FHIB. Figure 6 shows the corresponding cross-sectional bright field images from which the interaction domain and the evolution of nanobubbles can be analyzed. Nanobubbles were absent at the dose of 0.008 nC/μm according to Fig. 6(a). With dose increasing from 0.023 to 0.038 nC/μm, in addition to the expansion of the amorphous area, nanobubbles began to appear and enlarge along with the rise of surface swelling, as shown in Figs. 6(b)–6(d). Meanwhile, it could be noticed from Fig. 4 that there was no swelling on the Si surface implanted by 30 keV FHIB with dose increasing from 0.003 to 0.012 nC/μm in the absence of bubbles, which indicated that the swelling of the silicon surface was accompanied with the formation of bubbles.

In order to study the relationship between damage and ion concentration further, the damaged area and the ion concentration depending on a dose at the beam energy of 12 and 30 keV are shown in Fig. 7. See the supplementary material for TEM images of samples at 30 keV (Fig. S1).[26] Here, the ion concentration was estimated by the dose divided by corresponding damage area for a single-pixel line irradiation. As expected, at the same ion dose, higher energy resulted in a larger damage area and, therefore, a smaller ion concentration. Nanobubbles appeared when the ion dose reached about 0.015 nC/μm at 12 keV [Fig. S3(b)] while it reached about 0.03 nC/μm at 30 keV [Fig. S2(c)] according to the experimental results.[26] Accordingly, the estimated thresholds of ion concentration for nanobubble generation at 12 and 30 keV were 6.07 and 4.36 ions/nm^3, respectively, which were of the same order of magnitude and close to each other. It was consistent with the previous work of Raineri *et al.,* where the ion concentration threshold of nanobubbles generation was proved to be nearly the same at different beam energies.[25] The threshold values were different from results in that work, which might result from different implantation methods. Thus, the threshold range for nanobubble generation in crystalline Si could be specified around 5.2 ions/nm^3 as shown in Fig. 7(b). It was reasonable to infer that the generation and growth of helium nanobubble were exactly dependent on the local ion concentration. Only when ion concentration approaches to a specific threshold, the nanobubbles appear, and higher local ion concentration leads to larger bubbles.

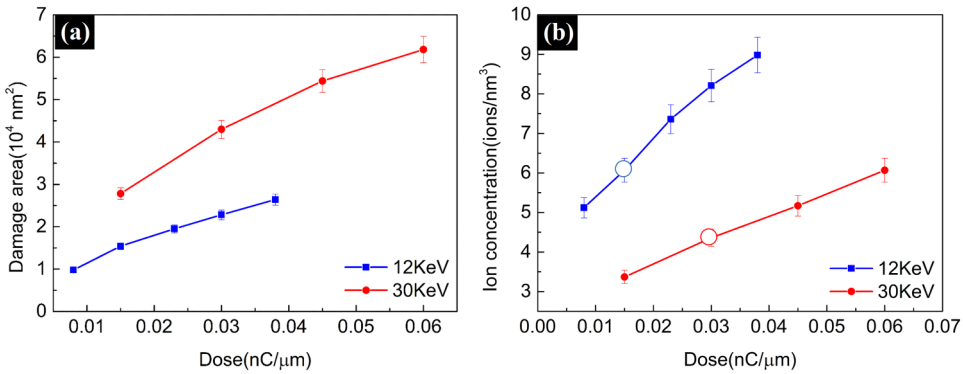

FIG. 7. (a) Damage area and (b) the ion concentration dependence on ion dose at 12 and 30 keV FHIB irradiation within a single-pixel line of 1 μm length, respectively. The circles in (b) mark the estimated threshold for nanobubble generation.

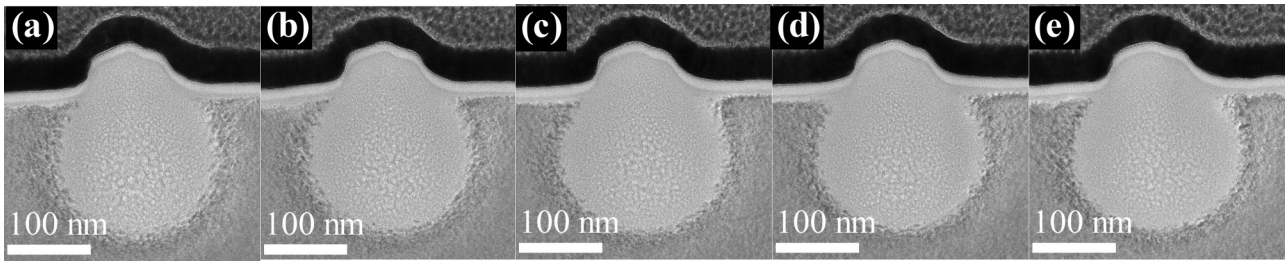

FIG. 8. High resolution TEM cross section of (111) silicon sample scanned as a single-pixel line with increasing beam current (a) 0.7, (b) 1.6, (c) 2.5, (d) 3.4, and (e) 4.3 pA at the beam energy of 12 keV and an ion dose of 0.05 nC/μm.

C. Beam current

Beam current represents the average dose delivery rate or instantaneous dose. For instance, a value of 1.0 pA means there will be 6.3 ions implanted per microsecond averagely. If the relaxation process in Si induced by previously injected ion would not interact with the following injected ion for implantations with low beam current, then the damage efficiency should remain the same. Nevertheless, the damage efficiency might be increased if the injecting beam current becomes large enough due to the consequent interactions between adjacent injecting paths. Here, in this work, when beam current varied from 0.7 to 4.3 pA by adjusting the helium gas pressure with fixed beam energy and dose of 0.05 nC/μm, there were no obvious differences in the morphology of damage domain. As Figs. 8(a)–8(e) shows, although damage area had a little tendency to increase with increasing beam current, the bubble distribution and bubble size were nearly the same among the implantation results with different beam currents. Thus, the beam currents introduced here were not enough to cause the interactions between adjacent ion injecting paths.

IV. CONCLUSION

In conclusion, we observed and investigated the process of the lattice damage and nanobubbles generation through a single-pixel spot and line irradiation of FHIB in single crystalline Si with varying ion dose, beam energies, and beam currents. The local ion concentration played a crucial role in the damage process. FHIB would create local defects and induce the amorphization process at low ion concentration. Once the ion concentration exceeds a certain threshold, helium nanobubbles could be generated. The bubble size would increase with ion concentration. This work provided a detailed and fundamental understanding about the interaction between FHIB and single crystalline Si and might help to promote the applications of HIM.

ACKNOWLEDGMENTS

The authors would like to thank Xujing Li for her GPA analysis support and Yun Huang for his work of eliminating oxide layer of silicon and Zongwei Xu for helpful discussion. This work was financially supported by the National Natural Science Foundation of China (NNSFC) (Nos. 11327902 11605001, and 11327902 51672007), the Ministry of Science and Technology of China (No. 2013YQ120353), and the "2011 Program" Peking-Tsinghua-IOP Collaborative Innovation Center of Quantum Matter.

[1]G. Hlawacek, V. Veligura, R. van Gastel, and B. Poelsema, J. Vac. Sci. Technol. B **32**, 020801 (2014).
[2]L. Scipioni, C. A. Sanford, J. Notte, B. Thompson, and S. McVey, J. Vac. Sci. Technol. B **27**, 3250 (2009).
[3]R. Livengood, S. Tan, Y. Greenzweig, J. Notte, and S. McVey, J. Vac. Sci. Technol. B **27**, 3244 (2009).
[4]D. Emmrich, A. Beyer, A. Nadzeyka, S. Bauerdick, J. C. Meyer, J. Kotakoski, and A. Gölzhäuser, Appl. Phys. Lett. **108**, 163103 (2016).
[5]Y. Deng, Q. Huang, Y. Zhao, D. Zhou, C. Ying, and D. Wang, Nanotechnology **28**, 045302 (2017).
[6]M. E. Schmidt, T. Iwasaki, M. Muruganathan, M. Haque, H. Van Ngoc, S. Ogawa, and H. Mizuta, ACS Appl. Mater. Interfaces **10**, 10362 (2018).
[7]J. Buchheim, R. M. Wyss, I. Shorubalko, and H. G. Park, Nanoscale **8**, 8345 (2016).
[8]D. S. Fox *et al.*, Nano Lett. **15**, 5307 (2015).
[9]M. M. Marshall, J. Yang, and A. R. Hall, Scanning **34**, 101 (2012).
[10]M. Aramesh, Phys. Status Solidi Phys. Rev. Lett. **12**, 1700333 (2018).
[11]V. Veligura, G. Hlawacek, R. P. Berkelaar, R. van Gastel, H. J. Zandvliet, and B. Poelsema, Beilstein J. Nanotechnol. **4**, 453 (2013).
[12]S. Hang, Z. Moktadir, and H. Mizuta, Carbon **72**, 233 (2014).
[13]S. Tan, K. Klein, D. Shima, R. Livengood, E. Mutunga, and A. Vladár, J. Vac. Sci. Technol. B **32**, 06FA01 (2014).
[14]M. G. Stanford, B. B. Lewis, V. Iberi, J. D. Fowlkes, S. Tan, R. Livengood, and P. D. Rack, Small **12**, 1779 (2016).
[15]M. G. Stanford, K. Mahady, B. B. Lewis, J. D. Fowlkes, S. Tan, R. Livengood, G. A. Magel, T. M. Moore, and P. D. Rack, ACS Appl. Mater. Interfaces **8**, 29155 (2016).
[16]M. Rudneva, E. V. Veldhoven, S. K. Malladi, D. Maas, and H. W. Zandbergen, J. Mater. Res. **28**, 1013 (2013).
[17]H. Zhang, Z. Liu, H. Wen, H. Xie, and C. Liu, Ultramicroscopy **171**, 34 (2016).
[18]L. Pizzagalli, M. L. David, and M. Bertolus, Model. Simul. Mater. Sci. Eng. **21**, 065002 (2013).
[19]G. F. Cerofolini, F. Corni, S. Frabboni, C. Nobili, G. Ottaviani, and R. Tonini, Mater. Sci. Eng. R Rep. **27**, 1 (2000).
[20]J. Guénolé, A. Prakash, and E. Bitzek, Appl. Surf. Sci. **416**, 86 (2017).
[21]E. Salvati, T. Sui, A. J. G. Lunt, and A. M. Korsunsky, Mater. Des. **92**, 649 (2016).
[22]E. Salvati, L. R. Brandt, C. Papadaki, H. Zhang, S. M. Mousavi, D. Wermeille, and A. M. Korsunsky, Mater. Lett. **213**, 346 (2018).
[23]Y.-C. Wang, D.-G. Xie, X.-H. Ning, and Z.-W. Shan, Appl. Phys. Lett. **106**, 081905 (2015).
[24]F. J. Yang, Atomic Physics, edited by J. Gao (Higher Education Press, Beijing, 2008), Vol. 4, pp. 14–21.
[25]V. Raineri, P. G. Fallica, G. Percolla, A. Battaglia, M. Barbagallo, and S. U. Campisano, J. Appl. Phys. **78**, 3727 (1995).
[26]See supplementary material at https://doi.org/10.1116/1.5096908 for the detailed evolution of nanobubbles at 30 KeV and 12 KeV beam energy with increasing dose.